LBL-11560 1/2c.2
Preprint

Lawrence Berkeley Laboratory
UNIVERSITY OF CALIFORNIA

Materials & Molecular
Research Division

Submitted to Acta Metallurgica

# CREEP FRACTURE IN CERAMIC POLYCRYSTALS
# I. CREEP CAVITATION EFFECTS IN POLYCRYSTALLINE ALUMINA

J.R. Porter, W. Blumenthal and A.G. Evans

September 1980

TWO-WEEK LOAN COPY

This is a Library Circulating Copy
which may be borrowed for two weeks.
For a personal retention copy, call
Tech. Info. Division, Ext. 6782.

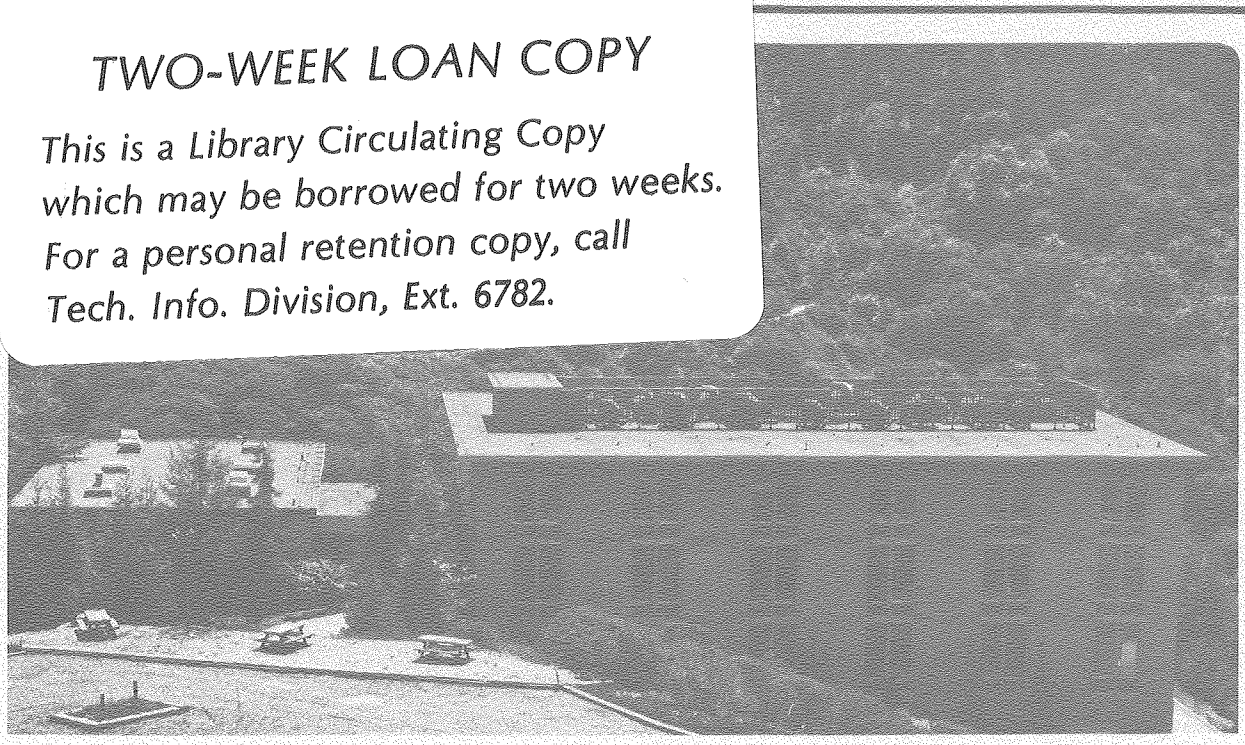

Prepared for the U.S. Department of Energy under Contract W-7405-ENG-48

LBL-11560 1/2 c.2

## DISCLAIMER

This document was prepared as an account of work sponsored by the United States Government. While this document is believed to contain correct information, neither the United States Government nor any agency thereof, nor the Regents of the University of California, nor any of their employees, makes any warranty, express or implied, or assumes any legal responsibility for the accuracy, completeness, or usefulness of any information, apparatus, product, or process disclosed, or represents that its use would not infringe privately owned rights. Reference herein to any specific commercial product, process, or service by its trade name, trademark, manufacturer, or otherwise, does not necessarily constitute or imply its endorsement, recommendation, or favoring by the United States Government or any agency thereof, or the Regents of the University of California. The views and opinions of authors expressed herein do not necessarily state or reflect those of the United States Government or any agency thereof or the Regents of the University of California.

# CREEP FRACTURE IN CERAMIC POLYCRYSTALS

## I. CREEP CAVITATION EFFECTS IN POLYCRYSTALLINE ALUMINA

by

J. R. Porter, W. Blumenthal and A. G. Evans

Materials and Molecular Research Division, Lawrence Berkeley Laboratory
and Department of Materials Science and Mineral
Engineering, University of California
Berkeley, CA 94720

## ABSTRACT

Fine grained polycrystalline alumina has been deformed in creep at high temperatures, to examine the evolution of cavities at grain boundaries. Cavities with equilibrium and crack-like morphologies have been observed, distributed non-uniformly throughout the material. The role of these cavities during creep has been described. A transition from equilibrium to crack-like morphology has been observed and correlated with a model based on the influence of the surface to boundary diffusivity ratio and the local tensile stress. The contribution of cavitation to the creep rate and total creep strain has been analyzed and excluded as the principal cause of the observed non-linear creep rate.

## 1. INTRODUCTION

The high temperature deformation of ceramics is frequently accompanied by the nucleation and growth of cavities at grain boundaries[1]. The presence of the cavities is evidently detrimental to the creep performance, since the cavities are both the ultimate origin of creep rupture[2] and a potential source of enhanced deformation. A detailed understanding of cavity evolution during creep is thus of paramount importance to the prediction of the high temperature performance of polycrystalline ceramics. Creep experiments which provide a basis for developing the requisite comprehension are described; experiments that include measurements of the deformation behavior and observations of the dominant cavity morphologies. The material selected for the study is a fine grained alumina, devoid of amorphous phases[†], for which the comprehensive diffusivity data needed to correlate the observations with cavitation models are available[3,4].

The measurements and the cavity observations are reported in the first section. The observations are then compared with the predictions of diffusive cavitation models, to establish the merit of such models for characterizing cavitation in this class of polycrystal. Finally, the models are used to examine the influence of cavitation on the creep deformation under various conditions of stress and temperature.

## 2. RESULTS AND OBSERVATIONS

Deformation tests were conducted on flexural specimens at constant displacement rates. The plastic strain levels achieved in the tests were determined from the separation of scribes placed on the side surface of

---

[†]The material was a hot pressed $Al_2O_3$/0.25% MgO with an average grain size of $\sim 2\mu m$.

the specimen[5]. In each test, steady state behavior (as manifest by a constant deformation load) was established, and it was ensured that the major contribution to the total strain was accrued in the steady state regime. The steady state deformation characteristics, deduced from the test results are summarized in figure 1. The strain rates, $\dot{\varepsilon}_\infty$, are typified by the conventional relation,

$$\dot{\varepsilon}_\infty \propto \sigma_\infty^n \exp [-Q/RT] \qquad (1)$$

where the exponent, $n$, of the applied stress, $\sigma_\infty$, is 1.8, and the activation energy $Q$ is $\sim$460 KJ/mole. Inspection of the data indicated that the deformation was not compatible with the existence of a stress threshold (a frequently invoked interpretation of exponents $n > 1$)[6,7]. The non-linearity of the deformation is presumed, therefore, to reside in the non-linearity of the dominant deformation mechanism. Grain growth occurred during the tests at the highest temperature (from $\sim$2μm to $\sim$4μm), but the change in structure was also excluded as the origin of the non-linearity, because incremental displacement rate tests (at constant structure) gave identical values for the stress exponent.

Most of the test specimens were subjected to an ultimate strain of 0.07, at the maximum outer fiber strain location. The specimens were then polished down to various levels beneath the surface in order to observe the cavity distributions created in the sample, as a function of the distance from the neutral axis. Appreciable cavity formation was invariably observed at the larger strain levels and, in all instances, the cavity distributions were inhomogeneous (figure 2): an observation of major significance to the interpretation of creep rupture. The cavity

morphologies and the cavitation strains exhibited some important trends with both the steady state stress level and the temperature. The influence of stress is demonstrated by comparing figures 2a and 2c, which indicate typical cavity distributions at a strain of 0.07, a test temperature of 1750 K and stresses of 80 and 8 MPa respectively. At the lower stress, the strain contributed by the cavities is $\sim$0.03 (i.e. $\sim$40% of the total plastic strain). The dominant morphology consists of equiaxed, triple point located cavities, as indicated by the schematic in figure 2d. These cavities are of essentially constant surface curvature and can thus be regarded as the equilibrium-shaped analogy of the lenticular diffusion created cavities frequently observed in metals on two grain junctions[9]. At the higher stress, the fraction of the total strain contributed by the cavities is smaller ($\sim$20%), and a substantial proportion of the cavities exhibit elongated morphologies. Closer examination indicated two characteristic elongated cavities; cavities that occupy an entire grain facet and cavities that extend partially across a grain facet, commencing from a triple point (figure 2b). The latter exhibit a tip morphology (figure 3) typical of crack-like cavities; cavities predicted to exist for conditions wherein relatively slow rates of surface diffusion limit the formation of an equilibrium shape[10]. These crack-like cavities presumably become stabilized in the form of facet-sized cavities after extending into the opposite triple junction (figure 2b). The tests at the lower temperatures, 1650K, exhibit the same characteristics, but there appears to be a reduced tendency for crack-like cavity formation at comparable stress levels, and a smaller net contribution to the strain from the cavitation. Regions in

which the crack-like cavities are aligned in essentially colinear arrays are also a frequent observation at the higher stress (figure 4a). In the zone of maximum strain (figure 4b) coalesced cavities are occasionally observed. These are undoubtedly the origin of microcracks and hence, are precursors to rupture.

Several specimens were fractured at room temperature following high temperature creep deformation, and the in-plane morphology of the cavities was examined. Some ellipsoidal cavities at these grain junctions were evident, but many of the cavities extended fully across the grain facet at the grain junctions. The cavity fronts generally exhibited a small monotonic curvature. There was no evidence of 'finger-like' cavity growth[11].

The grain boundaries were examined before and after deformation by employing TEM and STEM techniques. Amorphous phases were not detected (either at two grain or three grain junctions) and no significant segregation of MgO at the grain boundaries could be identified within the STEM resolution capabilities. Spinel particles were also an infrequent occurrence. Most grain boundaries were featureless, but a small fraction ($\sim$0.1) exhibited periodic structures (figure 5) similar to those observed by Carter et al[12].

## 3. DISCUSSION

The deformation measurements and the cavity observations indicate several important behavioral trends. The first significant observation is the inhomogeneous nature of the cavity distribution, particularly at the larger stress levels. This non-uniformity derives from the influence of material inhomogeneity in the nucleation and initial growth of the

cavities. The evolution of inhomogeneous cavity arrays and the resultant creation of macrocracks is the principal theme of the companion paper[8].

Probable sources of inhomogeneity are local variability in the dihedral angle or the diffusivity along the cavity surfaces (such that small values of these parameters encourage cavity extension[8]). Boundaries with periodic structures (figure 5) are, for example, likely to exhibit larger dihedral angles than the general boundary and it is, perhaps, significant that such boundaries have not been observed to contain cavities. Boundaries with an excess of impurity species in solid solution (MgO or $SiO_2$) could exhibit the smaller than average diffusivities or dihedral angles needed to encourage local cavitation.

The transition from equilibrium to crack-like cavities at high stresses is a phenomenon with substantial implications. An analysis of the transition, recently proposed by Chuang et al.[13], indicates a limit on equilibrium cavity growth imposed by the ratio of the surface diffusivity to the grain boundary diffusivity. Implicit in the occurrence of a transition is the existence of diffusive crack-like cavities with a near tip morphology that is essentially independent of the initial equilibrium cavity shape[12].

In the following sections, a detailed analysis of observed crack-like cavity morphologies is conducted, in order to establish credence in the transition model. Finally, the influence of the cavitation on the creep strain is examined, with emphasis on the deviations from linearity introduced by the cavitation.

*3.1 The Cavity Shape*

The near-tip shape of crack-like cavities created by diffusion is dictated primarily by the surface diffusivity of the material and the cavity velocity, but relatively independent of the initial, equilibrium cavity shape[13,14]. The specific shapes of observed crack-like cavities (figure 6) are thus examined in detail in order to determine the level of conformance with the predictions of the diffusive cavity growth model. (The cavity profiles are used for the shape investigation, by assuming in each case that the cavity fronts exhibit a small monotonic curvature: rather than the sinusoidal shape characteristic of finger-like growth. The observed cavity fronts are consistent with this assumption. Also, computations of the critical wavelength for the growth of a perturbation[11] indicate values > 2μm, i.e. of the order of the grain facet length, which is too large to permit finger development under the present test conditions). An explicit prediction of the model is an expression for the cavity width $w$ in the fully established crack-like growth model[13],

$$w^3 = 8 \frac{D_s \delta_s \gamma_s \Omega}{kTv} \left[2\left(1 - \frac{\cos\Psi}{2}\right)\right]^{3/2} \qquad (2)$$

where $D_s\delta_s$ is the surface diffusion parameter, $\gamma_s$ is the surface energy, $\Omega$ the atomic volume, $\Psi$ the dihedral angle and $v$ is the steady-state cavity tip velocity. The rate of propagation of the cavities in the crack-like mode is approximately constant[8,15] (See Appendix). Cavity shape analysis has thus been confined to well developed crack-like cavities. A typical example is the cavity shown in figure 6a. An upper bound $\hat{w}$ on the width of such fully developed cavities is predicted from eqn. (2) by assuming

that the cavities have been extending continuously, at constant velocity, from the initial attainment of steady-state deformation. Measurements of the dihedral angle obtained from several cavities indicate that $\Psi = 83°$. By adopting this value for the dihedral angle and by introducing previously determined values[3,4] for other parameters (at 1650K, $D_s\delta_s = 2.5 \cdot 10^{-21} m^2 s^{-1}$, $\Omega = 2.2 \cdot 10^{-30} m^3$, $\gamma_s = 0.9 Jm^{-2}$) the upper bound cavity width, $\hat{w}$, can be predicted. For the cavity shown in figure 6 the upper bound value of the cavity width is 224 nm, compared with a measured width of 90 nm. For each case, examined in this way, the measured width was always less than the upper bound value and within a factor of 3. Considering the uncertainty in the diffusion parameter, these correspondences are considered to be sufficiently close to confirm that the observed crack-like cavities had indeed formed by a diffusive mechanism, with surface diffusion as the rate limiting step.

*3.2 The Transition*

The transition from the equilibrium to crack-like cavity morphology is dependent upon the stress level, the relative cavity size and the ratio $\Delta$ of the surface to boundary diffusivities[8,13]. The location of this transition is plotted in figure 7 for a temperature of 1550K ($0.15<\Delta<0.5$)[3]. The experimentally observed cavities can be placed on the transition diagram to examine conformance with the prediction. This is achieved by adopting the following procedure. Colinear arrays of crack-like and equilibrium cavities nearly normal to the strain axis are identified (e.g. from figures 2 and 4). The cavity size ratio within the array is determined by direct measurement and the position on the transition diagram is located and plotted. The results are indicated on figure 7 for results obtained at 1550K; open

circles represent arrays of equilibrium-shaped cavities and closed circles refer to crack-like arrays. At this temperature, the predicted transition line adequately separates the experimental observations of the two cavity types. However, at other temperatures, the model was less successful.

The reasonable correlations of both the predicted crack-like cavity shapes and the transition condition with the present observations lend credence to the diffusive model as a quantitative description of the cavitation process in fine-grained $Al_2O_3$. It is appropriate, therefore, to examine the influence of diffusive cavitation on the creep deformation, implied by the cavity growth models.

### *3.3 Creep Deformation*

When cavities develop during creep deformation, the deformation rate is inevitably enhanced. It is important to ascertain the extent of this enhancement under various conditions of imposed stress and temperature and to identify influences upon the stress exponent of the deformation rate. The non-linearity will be firstly examined by applying the relations for the creep strain induced by the various cavitation processes derived in the Appendix. The creep strain rate relations for cavitation have been derived for uniform cavity arrays. It is noted that these must be upper bound estimates for inhomogeneous cavitation, because of growth constraints imposed by the creep rate of the surrounding non-cavitated structure[8].

The influence of cavitation on the non-linearity of creep in the present test is found to be minimal. This can be appreciated by noting that the only non-linear strain rate relation is that which pertains during the extension of crack-like cavities at low stress levels: a process for which $\dot{\varepsilon} \propto \sigma^2$.

Yet, inspection of the cavity morphologies at any instant during the deformation process (figure 2a) indicates that the fraction of cavities propagating in the crack-like mode is relatively small (5 to 20%). Hence, since the total strain contribution from the cavities is <30%, it is implausible to anticipate a creep exponent in the presence of cavitation that exceeds $\sim$1.2. The observed non-linearity of the creep rate, $n \sim 1.8$, is thus concluded to originate primarily from a non-linear creep mechanism. The most likely origin of the non-linearity resides in 'interface' limitations; effects concerned with the vacancy creation/annihilation process at grain boundaries, or with impediments to grain boundary sliding (as yet, unspecified)[16]. It is tempting to invoke the non-linearities contained in dislocation models of grain boundary creep[17]. But, it is difficult to envisage on the basis of the present observations that a sufficient fraction of boundaries can be described by a discrete dislocation array to permit such models to be applied with confidence. This is clearly an issue that merits further investigation.

The extent of the deformation attributed to the cavitation can be predicted from models of uniform cavity arrays. The predictions are summarized in figure 8, in terms of the parameter $R$, the cavitation creep rate relative to the Coble creep rate and $f$, the ratio of the crack length to crack spacing. For a typical value of $\Delta$ ($\Delta = 1$), figure 8 shows that the proportion of the cavitation creep attributed to the growth of crack-like or full-facet cavities is less than that derived from equilibrium shaped cavities, by a factor of $\sim$3. This prediction is in substantial

agreement with the observations summarised in figure 2. However, a quantitative correlation between theory and experiment would be considerably complicated by the mixture of cavity morphologies typically observed, and the resultant tendency for the development of local constraints. Additional study is thus needed before the contributions of cavitation to the deformation can be adequately predicted.

## 4. CONCLUSIONS

Non-linear creep behavior ($n \sim 1.8$) has been observed in a fine grained hot-pressed, polycrystalline $Al_2O_3$/0.25% MgO. At all stress levels, cavities were observed to nucleate at grain triple junctions. At lower stress levels, creep cavities were predominantly equiaxed; whereas at higher stress levels, cavities frequently evolved into crack-like configurations and subsequently extended fully across the grain facets. However, the proportion of the creep strain attributable to cavitation was higher in the specimens deformed at the lower stress levels. Under all testing conditions, the cavitation was inhomogeneous and cavity coalescence was encountered at large strains. Such behavior was attributed to variability in the dihedral angle or the surface diffusivity.

The observed crack-like cavity shapes and the transition from equilibrium to crack-like morphology was shown to be consistent with models of diffusive cavity growth that allow changes in cavity shape when the surface diffusivity becomes too small to maintain uniform curvature. This correlation has important implications for the prediction of creep rupture[8].

The contribution to the total creep strain was derived for three different arrays of cavities. Each model predicted linear behavior at the stress levels used in the present creep tests, discounting cavitation as the source of the observed non-linearity (a common misconception). The non-linearity is thus attributed to the actual deformation mechanism (i.e., interface limitations or grain boundary sliding thresholds).

REFERENCES


1. R. C. Folweiler, Creep Behavior of Pore Free Polycrystalline Aluminum Oxide, J. Appl. Phys., 32: 773 (1961).
2. A. G. Evans and A. Rana, High Temperature Failure Mechanisms in Ceramics, Acta Met., 28: 129 (1980).
3. J. M. Dynys et al., Mechanisms of Atom Transport during Initial Stage Sintering of $Al_2O_3$, in: "Sintering Processes," G. C. Kuczynski, ed., Plenum, New York (1980).
4. R. M. Cannon and R. L. Coble, Review of Diffusional Creep of $Al_2O_3$, in: "Deformation Mechanisms in Ceramics," R. C. Bradt and R. E. Tressler, eds., Plenum, New York (1975).
5. W. Blumenthal, M. S. Thesis, U. of California, Berkeley (1980).
6. M. F. Ashby and R. A. Verall, Diffusion-Accomodated Flow and Superplasticity, Acta Met., 21: 149 (1973).
7. B. Burton, Interface Reaction Controlled Diffusion Creep, Mat. Sci. Eng., 10: 9 (1972).
8. C. H. Hsueh and A. G. Evans, Creep Fracture in Ceramic Polycrystals II. Effect of Inhomogeneity on Creep Rupture; to be published.
9. R. Raj and M. F. Ashby, Intergranular Fracture at Elevated Temperature, Acta Met., 23: 653 (1975).
10. T-J Chuang and J. R. Rice, The Shape of Intergranular Creep Cracks Growing by Surface Diffusion, Acta Met., 21: 1625 (1973).
11. R. J. Fields and M. F. Ashby, Finger-like Crack Growth in Solids and Liquids, Phil. Mag. 33 (1976) 33.
12. C. B. Carter, D. L. Kohlstedt and S. L. Sass, Electron Diffraction and Microscopy Studies of the Structure of Grain Boundaries in $Al_2O_3$, Materials Science Center Report #4152, Cornell Univ., Ithaca, New York (1979).

13. T-J Chuang et al., Non-equilibrium Models for Diffusive Cavitation of Grain Interfaces, Acta Met., 27: 265 (1979).

14. G. M. Pharr and W. D. Nix, A Numerical Study of Cavity Growth Controlled by Surface Diffusion, Act Met., 27: 1615 (1979).

15. A. G. Evans, J. R. Rice and J. P. Hirth, Suppression of Cavity Formation in Ceramics: Prospects for Superplasticity, J. Am. Ceram. Soc., 63: 368 (1980).

16. R. M. Cannon, W. H. Rhodes and A. H. Heuer, Plastic Deformation of Fine-Grained Alumina ($Al_2O_3$): I, Interface-Controlled Diffusional Creep, J. Am. Ceram. Soc., 63: 46 (1980).

17. T. G. Langdon, Grain Boundary Sliding as a Deformation Mechanism during Creep, Phil. Mag., 22: 689 (1970).

## ACKNOWLEDGMENT

The authors wish to thank J. R. Rice, B. B. Carter and R. M. Cannon for useful discussions. This work was supported by the Division of Materials Sciences, Office of Basic Energy Sciences, U. S. Department of Energy under contract No. W-7405-Eng-48.

## APPENDIX

## DEFORMATION RATES DUE TO CAVITATION

Deformation can occur due to the growth of cavities in a creeping structure. When the cavity distributions are in the form of uniform arrays, the cavity induced deformation can be superimposed onto the general creep deformation to obtain an approximate measure of the total creep strain. More complex behavior pertains in the presence of appreciable inhomogeneity. Deformation rates can be deduced for each of the following cavity morphologies; the expansion of equilibrium cavities, the extension of crack-like cavities and the thickening of full facet-sized cavities. The results for each will be compared with the creep rate due to grain boundary diffusion, as a basis for estimating their relative importance.

### 1. Equilibrium cavities

The deformation induced by equilibrium-shaped triple point cavities is given by[8];

$$\dot{\delta} = \left(\frac{3D_b\delta_b\Omega}{kTb^2}\right) \frac{[\sigma_\infty - (1-f)\sigma_o]}{(1-f)^3} \qquad (A1)$$

where $f = a/b$, $\dot{\delta}$ is the rate of separation of adjacent grains due to the deposition of matter (from the cavities) onto the intervening grain boundaries and $\sigma_o$ is the sintering stress,

$$\sigma_o = \gamma_s h(\Psi)/a$$

where $h(\Psi)$ is a function that depends on the dihedral angle. The sintering stress is only significant immediately after nucleation when $a$ is very small. Thereafter, it can be effectively neglected. Then, for $f \lesssim 0.3$, typical of the present observations, eqn. (A1) reduces to;

$$\dot{\delta} = \left(\frac{3D_b\delta_b\Omega}{kTb^2}\right)\frac{\sigma_\infty}{(1-f)^3} \qquad (A3)$$

The ratio of the deformation rate to that for Coble creep is thus;

$$R_{equ} = \frac{3}{14\pi}\left(\frac{g}{b}\right)^2\frac{1}{(1-f)^3} \qquad (A4)$$

where $g$ is the grain diameter. This ratio is plotted in figure 9 for a cavity located at each triple point ($g \sim \sqrt{2}\, b$).

2. Crack-like cavities

The deformation rate induced by an array of colinear crack-like cavities can be derived from the expression for the velocity,

$$\nu^{2/3}(16/3)(1-f)^3\Delta + \nu^{1/3}\,2(1-f) = [\sigma_\infty b/\gamma_s \sin(\Psi/4)] \qquad (A5)$$

where $\nu = vkTb^3/D_s\delta_s\gamma_s\Omega$, and for the deformation[13]

$$\dot{\delta} = 4\,\nu^{2/3}\left(\frac{D_s\delta_s\gamma_s\Omega}{kTb^3}\right)\sin(\Psi/4) \qquad (A6)$$

Substituting $\nu$ from eqn (A6) into eqn (A5) two solutions obtain for the deformation rate. At low stress, $\sigma_\infty b/\gamma_s < 1$,

$$\dot{\delta} = \frac{(\sigma_\infty b/\gamma_s)^2}{(1-f)^2[\sin(\Psi/4)]}\left(\frac{D_s\delta_s\gamma_s\Omega}{b^3}\right) \qquad (A7)$$

This is the only result that yields non-linear behavior. However, the stress level at which this deformation rate pertains is lower than that employed in the present tests and generally too low to be of practical significance. At

higher stresses, $\sigma b/\gamma_s > 10$,

$$\dot{\delta} = \frac{3\sigma_\infty}{4b^2(1-f)^3} \left(\frac{D_s \delta_s \Omega}{kT}\right) \tag{A8}$$

The ratio of this creep rate to that for Coble creep is thus;

$$R_{crack} \left(\frac{0.05}{\pi}\right)\left(\frac{g}{b}\right)^2 \frac{\Delta}{(1-f)^3} \tag{A9}$$

This result is also plotted in figure 9 for $g \approx \sqrt{2}\, b$ for a typical $\Delta$ of 1.

3. Facet sized cavities

The deformation rate induced by an array of full facet cavities, shown schematically in figure 9a, growing by surface diffusion can be derived if the cavity shape remains fixed, and the surface tangent is relatively position invariant. The surface flux along the cavity, due to its curvature, is given by;

$$J_s = - \frac{D_s \delta_s}{kT\,\Omega} \left(\frac{d\mu}{dx}\right) \tag{A10}$$

and $\mu = \gamma_s \Omega / r$ where $r$ is the radius of the curvature of the surface.

To conserve matter the velocity of the cavity surface in the direction of the applied tensile stress is

$$\dot{y} = - \Omega \frac{dJ_s}{dx} \tag{A11}$$

Combining eqns. (A10) and (A11) and noting that the curvature, $1/r$, is $\sim d^2y/dx^2$ we obtain

$$\dot{y} = \frac{D_s \delta_s \Omega \gamma_s}{kT} \left(\frac{d^4 y}{dx^4}\right) \tag{A12}$$

This integral equation can be solved for steady-state conditions (constant $\dot{y}$) subject to the boundary conditions; (i) the flux at the cavity center is zero (i.e., $d^3y/dx^3 = 0$ at $x = 0$), (ii) the cavity is symmetric about its center (i.e., $dy/dx = 0$ at $x = 0$) and (iii) that the cavity shape at the intersection with the grain boundary must satisfy the dihedral angle requirements (i.e., at $x = a$ $dy/dx$ is $\tan[\Psi/2 - \pi/3]$). The solution for the surface curvature of the cavity is;

$$\frac{1}{r} \approx \frac{d^2y}{dx^2} = \frac{[3x^2-a^2]kT\dot{y}}{6D_s\delta_s\gamma_s\Omega} + \frac{\tan[\Psi/2-\pi/3]}{a} \qquad (A13)$$

The surface curvature ($1/r_o$) at the grain boundary intersection point ($x=a$) is,

$$\frac{1}{r_o} \approx \frac{kT\dot{y}a^2}{3D_s\delta_s\gamma_s\Omega} + \frac{\tan[\Psi/2-\pi/3]}{a} \qquad (A14)$$

The stress along the grain boundary separating adjacent cavities is dictated by the grain boundary diffusivity and the level of the applied stress. For uniform thickening between cavities, the stress is characterized by the relation[2];

$$\frac{d^2\sigma(x)}{dx^2} = \frac{\dot{\delta}kT}{D_b\delta_b\Omega} \qquad (A15)$$

where x is now measured from the center of the grain facet. This differential equation can be solved subject to the boundary conditions; (i) the flux at the grain facet center is zero ($d\sigma/dx = 0$ at $x = 0$) and (ii) the stress at the cavity intersection must be continuous ($\sigma = \gamma_s/r_o$ at $x = b - a$). The solution is;

$$\sigma(x) = \gamma_s/r_o + \frac{\dot{\delta} kT}{2D_b\delta_b\Omega} \left[(b-a)^2 - x^2\right] \tag{A16}$$

The average stress over the intervening facet is thus;

$$\langle\sigma\rangle = 1/(b-a)\int_0^{(b-a)} \sigma(x)dx$$

$$= \gamma_s/r_o + \frac{\dot{\delta} kTb^2}{3D_b\delta_b\Omega} (1-f^2) \tag{A17}$$

This is related to the applied stress by;

$$\langle\sigma\rangle = \sigma_\infty/(1-f) \tag{A18}$$

The displacement rate thus becomes;

$$\dot{\delta} = \frac{3D_b\delta_b\Omega}{kTb^2(1-f)^2} \left[\frac{\sigma_\infty}{(1-f)} - \frac{\gamma_s}{r_o}\right] \tag{A19}$$

Conservation of matter requires that;

$$\dot{y} = \dot{\delta}/2f \tag{A20}$$

The final expression for the thickening rate deduced from eqns. (A14), (A19) and (A20) is thus;

$$\dot{\delta} = \left(\frac{3D_b\delta_b\Omega}{kTb^2}\right) \frac{\left[\sigma_\infty - (\gamma_s/a)\tan[\Psi/2 - \pi/3]\right]}{(1-f)^3[1 + f/2(1-f)^2\Delta]} \tag{A21}$$

The ratio with respect to Coble creep for a typical stress level ($\sigma >> \gamma_s/a$) is then;

$$R_{facet} = \left(\frac{3}{7\pi}\right)\left(\frac{g}{b}\right)^2 \frac{\Delta}{(1-f)[f + 2\Delta(1-f)^2]} \tag{A22}$$

The growth of full-facet cavities differs from that for the other cavity

morphologies in that the relative spacing f remains invariant during the deformation. The choice of b, g and f are thus interrelated. Some typical results ($f = 0.5$, $b = g$; $f = 0.25$, $b = 2g$) are plotted in figure 9 for $\Delta = 1$.

# FIGURE CAPTIONS

Figure 1. Creep data for hot pressed alumina deformed in a 3 point bend mode. Stress exponent, n = 1.8.

Figure 2. Cavity shapes and distributions after deformation at high and low stress levels.

a. SEM image of section showing crack-like and full facet cavities.

b. Schematic of crack-like and full facet cavities.

c. SEM image of section showing equilibrium shaped cavities, $\sigma$ = 8 MPa, T =1750K.

d. Schematic of equilibrium shaped cavities.

Figure 3. TEM of crack-like cavity showing Chuang and Rice growth behavior. $\sigma$ = 60MPa. T = 1750K.

Figure 4. Arrays of crack-like and full facet cavities.

a. TEM image of colinear crack like cavities. $\sigma$ = 80MPa, T = 1750K.

b. SEM image of coalesced full facet cavities, $\sigma$ = 40MPa, T = 1750K.

Figure 5. An example of a grain boundary exhibiting periodicity.

Figure 6. A crack-like cavity.

a. TEM image, $\sigma$ = 100 MPa, T = 1750K.

b. Schematic.

Figure 7. Cavity transition diagram. Crack-like cavities are predicted above the shaded region, equilibrium cavities below. ● represents observation of crack-like cavities. ○ represents observations of equilibrium cavities. The shaded region corresponds to the solution of equation (3) for $0.15 < \Delta < 0.5$.

Figure 8. Cavity deformation ratio diagram relative to Coble creep for the diffusive growth of equilibrium, crack-like and full facet cavities for $\Delta = 1$.

Figure 9. Schematic diagram of full facet cavity array model

a. Cavity array.

b. Individual full facet cavity.

c. Stress distribution along linking boundary.

d. Cavity tip geometry.

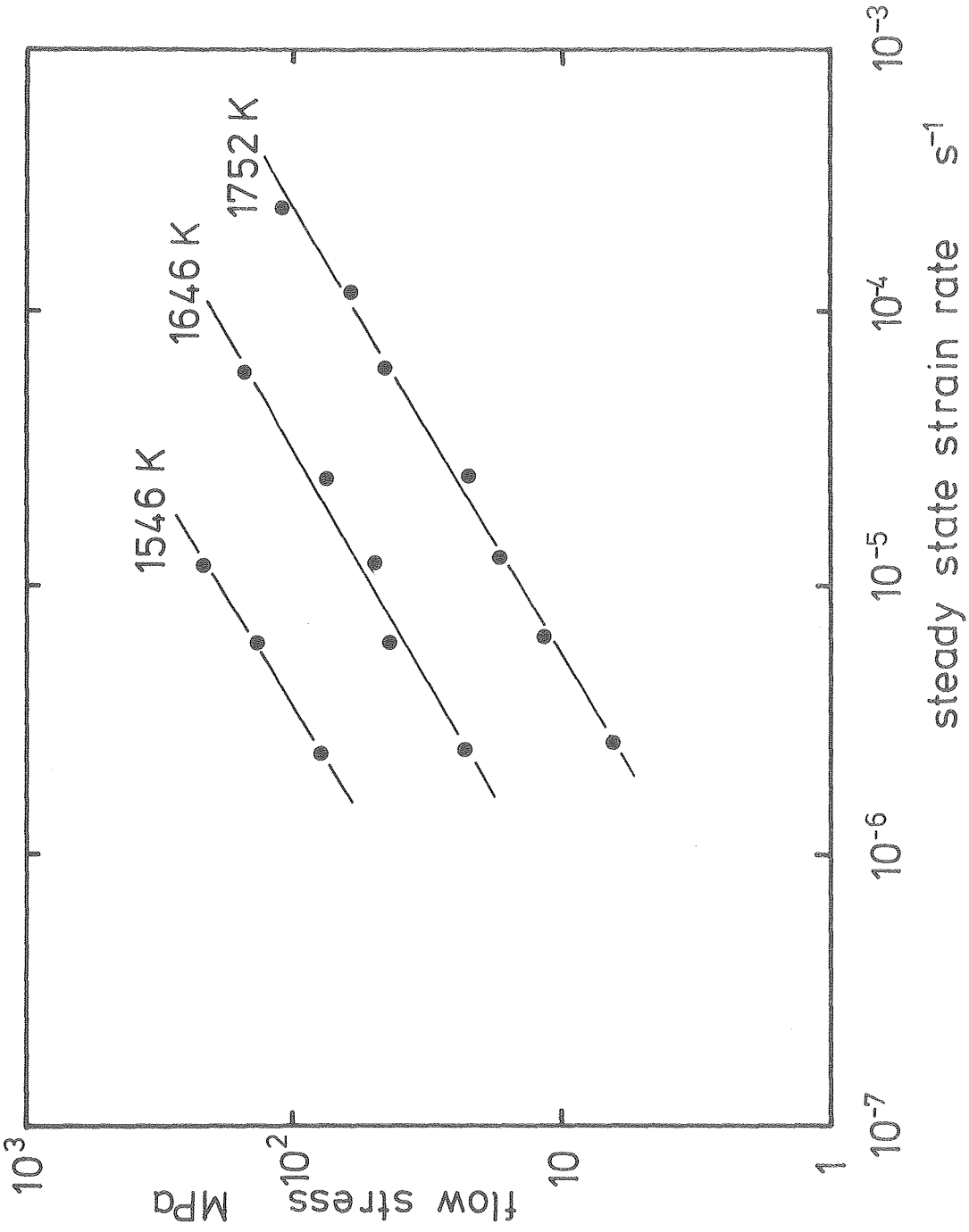


XBL 804-9364

Fig. 1

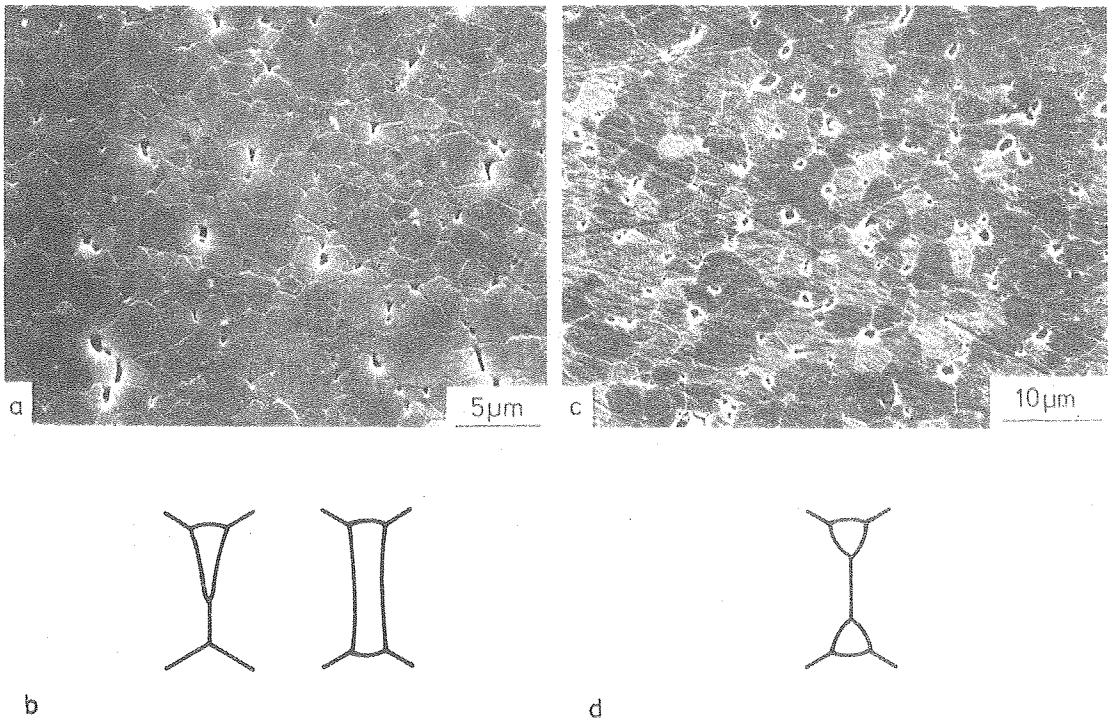


XBB 809-11137

Fig. 2

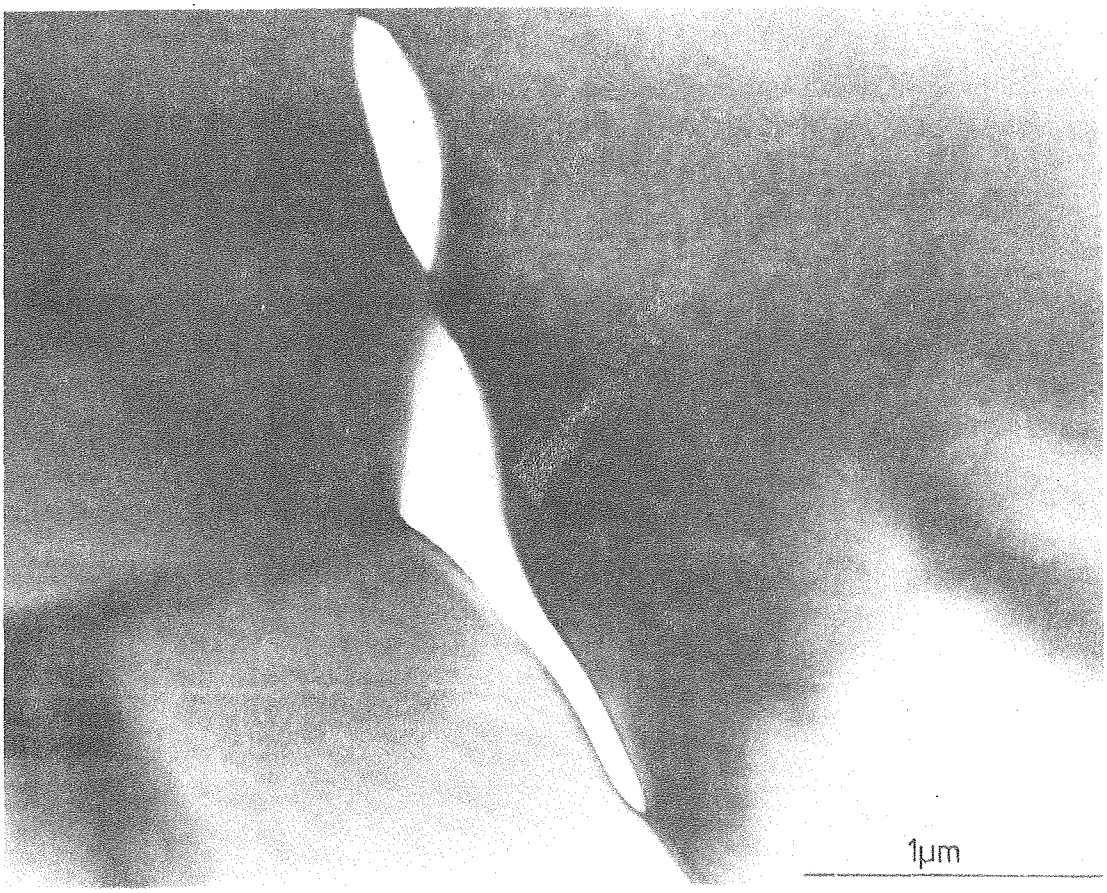


XBB 804-4971

Fig. 3

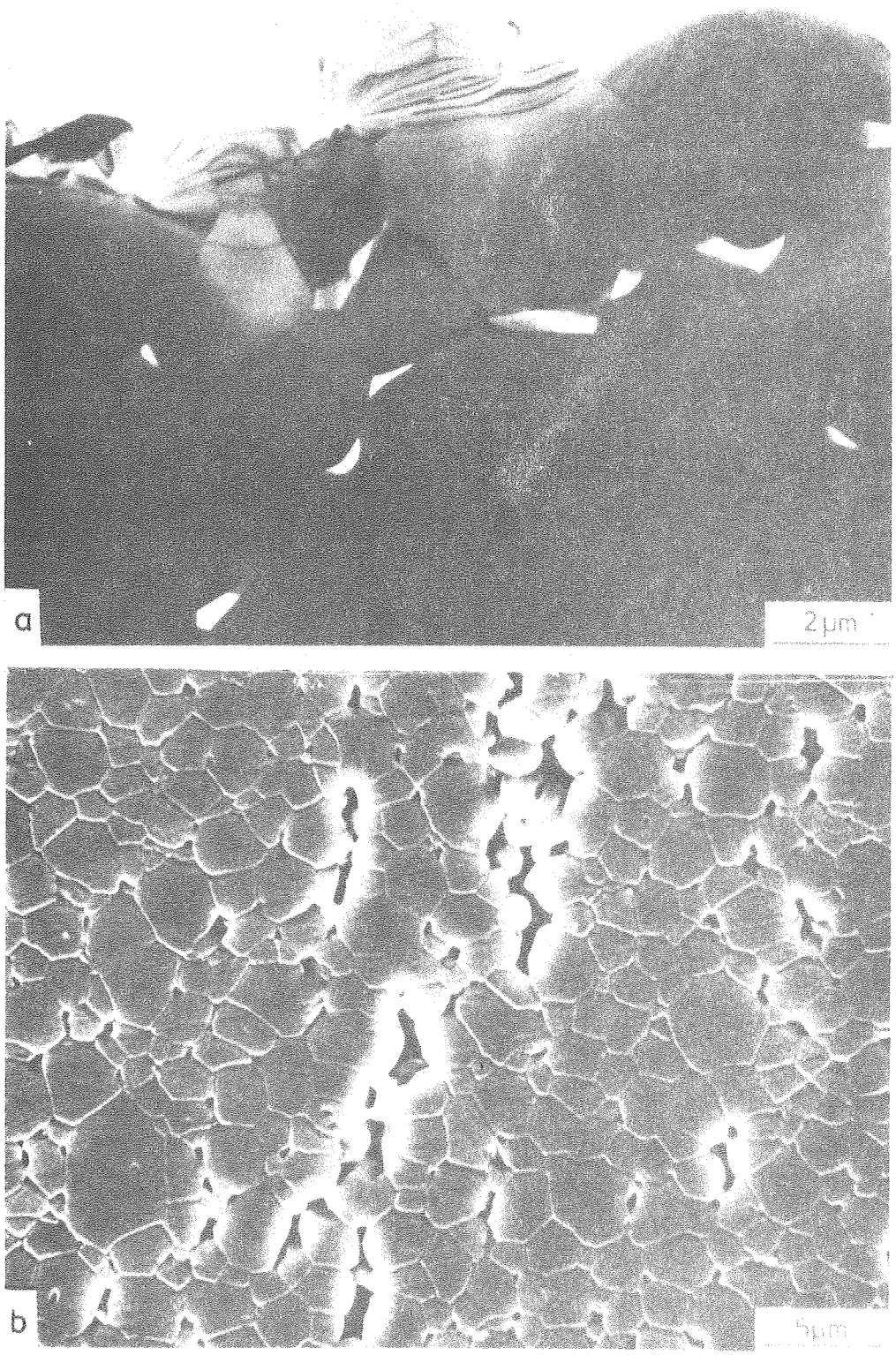


XBB 809-11135

Fig. 4

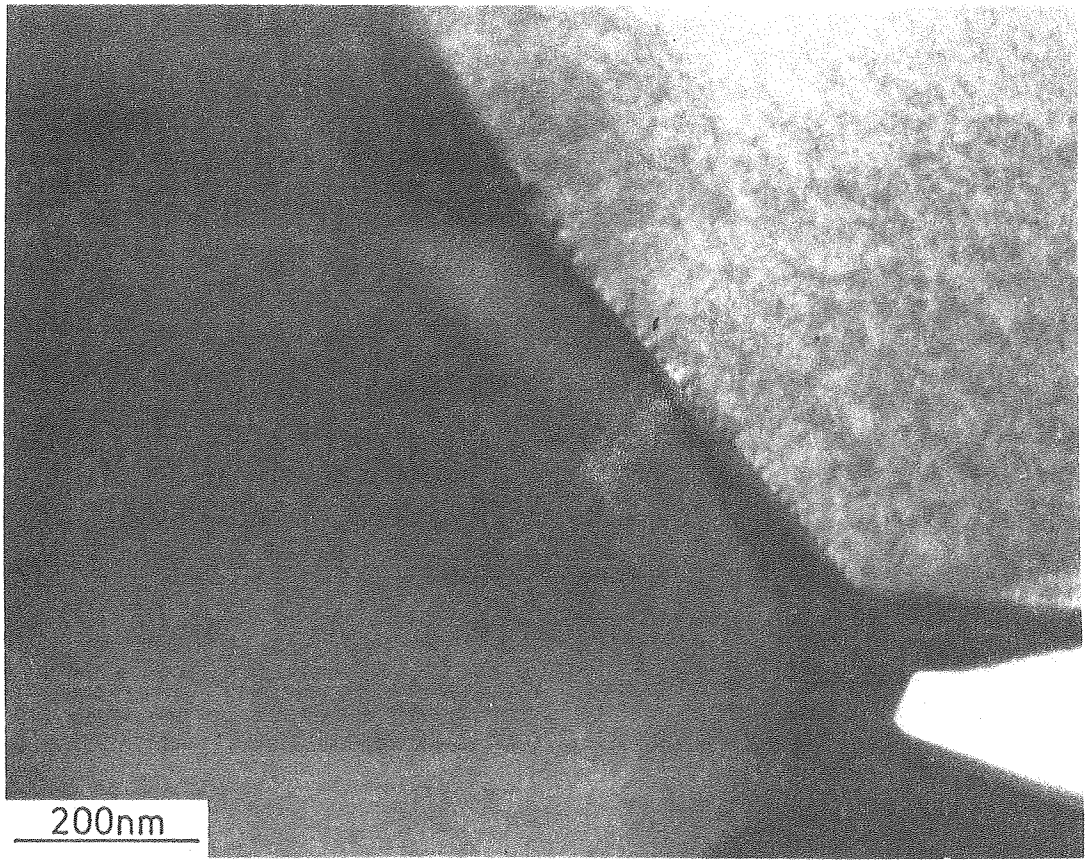


Fig. 5

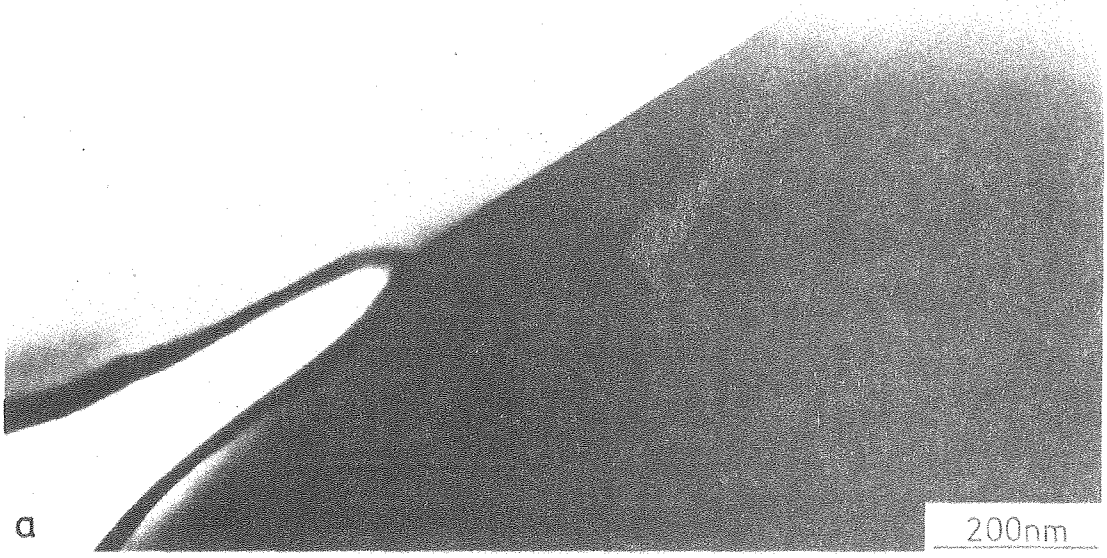


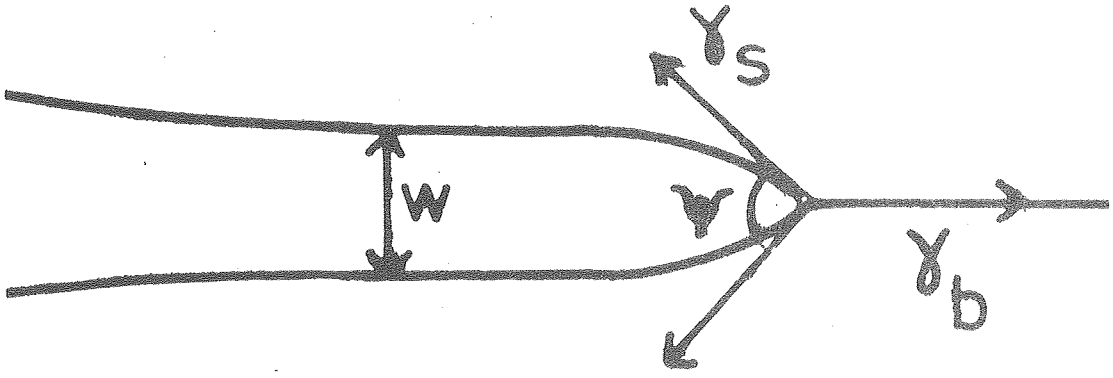


XBB 809-11136

b

Fig. 6

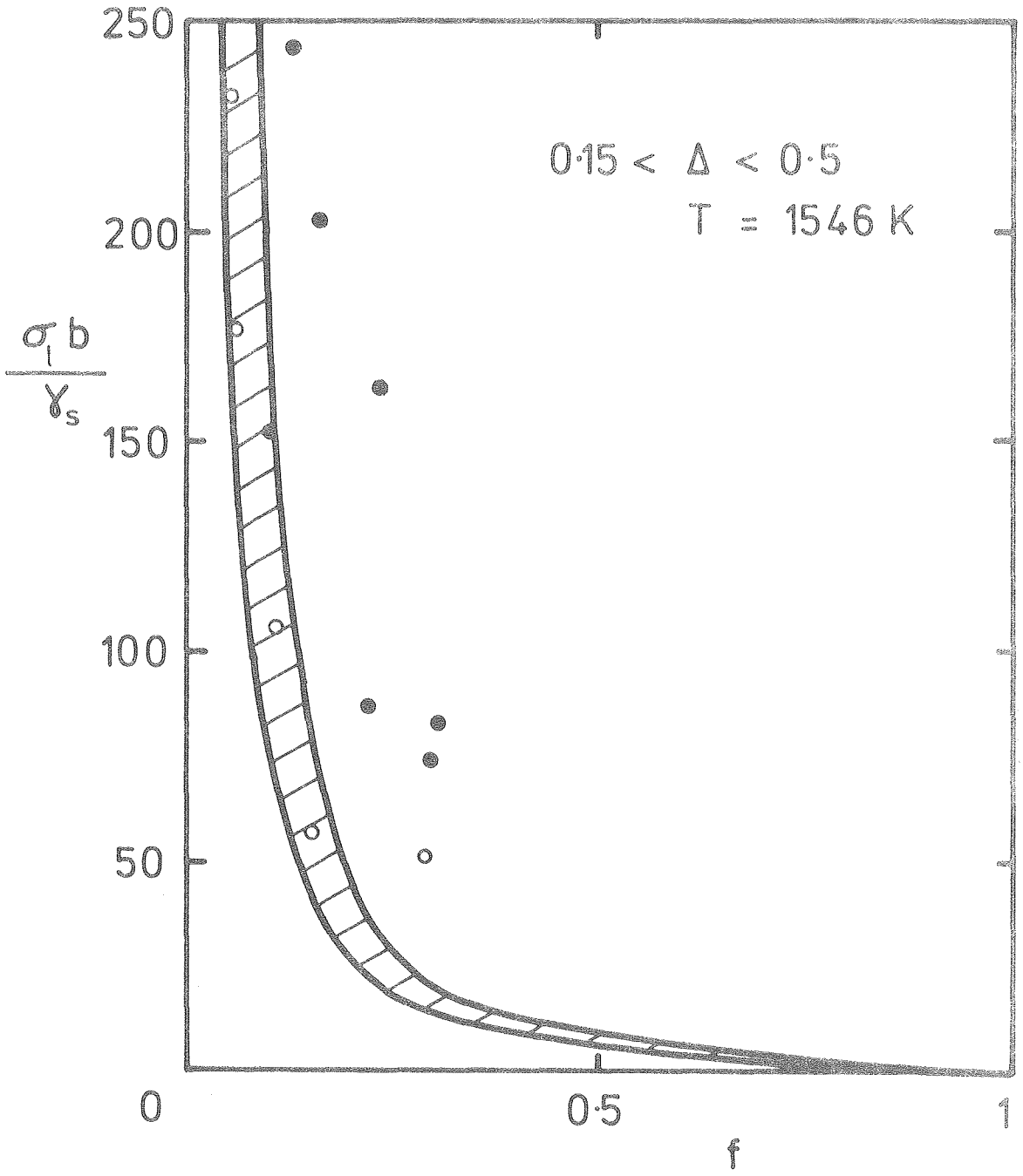


Fig. 7

XBL 808-11538

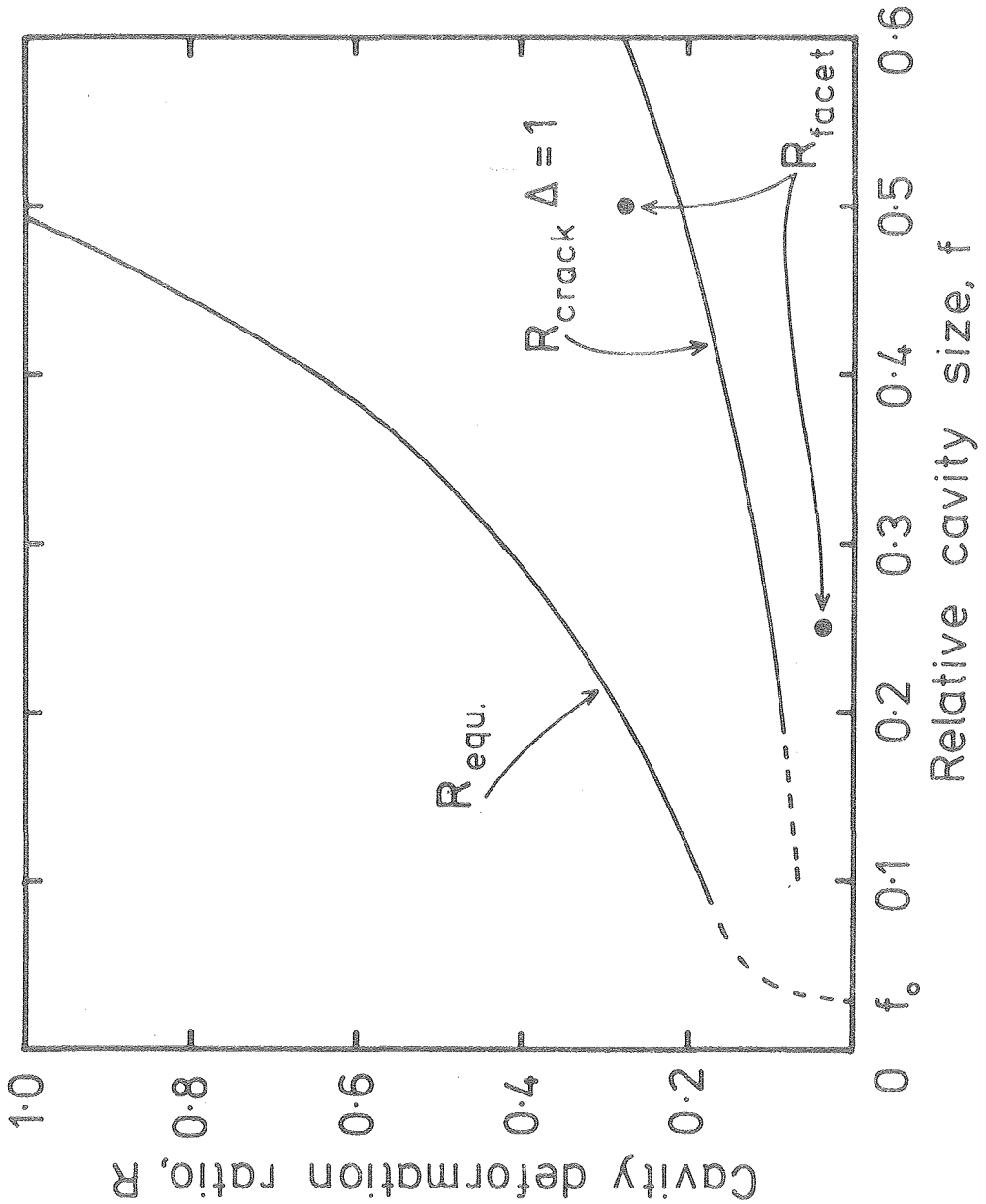


XBL 809-11903

Fig. 8

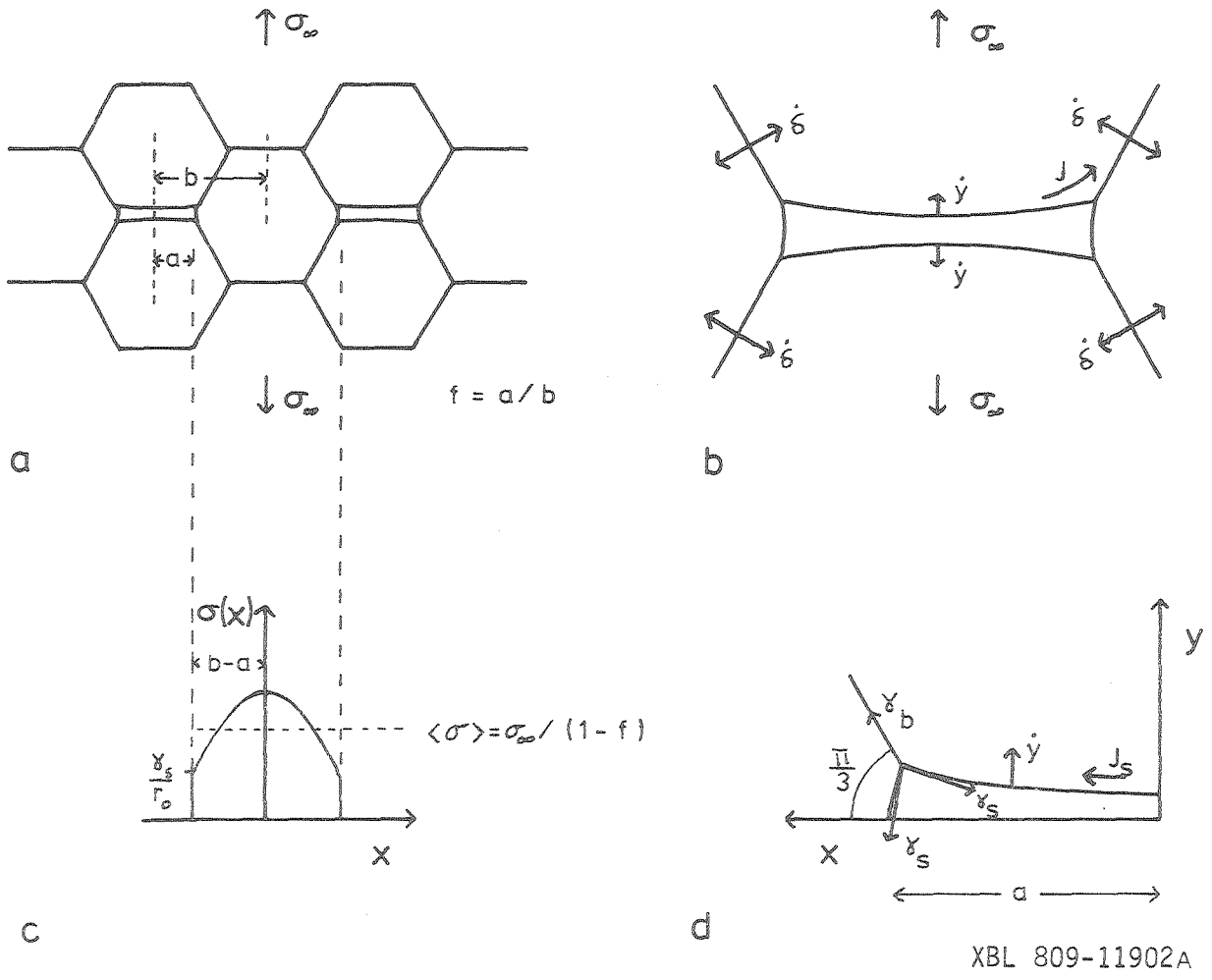


XBL 809-11902A

Fig. 9